


6-2019

Modulation of Biological Responses to 2 ns Electrical Stimuli by Field Reversal

Esin B. Sözer

P. Thomas Vernier

Follow this and additional works at: https://digitalcommons.odu.edu/bioelectrics_pubs

 Part of the [Biochemistry Commons](#), [Biomedical Engineering and Bioengineering Commons](#), [Biophysics Commons](#), and the [Molecular Biology Commons](#)



ELSEVIER

Contents lists available at ScienceDirect

BBA - Biomembranes

journal homepage: www.elsevier.com/locate/bbamem

Modulation of biological responses to 2 ns electrical stimuli by field reversal

Esin B. Sözer*, P. Thomas Vernier

Frank Reidy Research Center for Bioelectrics, Old Dominion University, 4211 Monarch Way Suite 300, Norfolk, VA 23508, USA

ARTICLE INFO

Keywords:

Electropermeabilization
 Membrane transport
 Membrane potential
 Bipolar electric pulse exposure
 Nanosecond electric pulse exposure
 YO-PRO-1
 Calcein
 Volume regulation
 Goldman-Hodgkin-Katz equation

ABSTRACT

Nanosecond bipolar pulse cancellation, a recently discovered phenomenon, is modulation of the effects of a unipolar electric pulse exposure by a second pulse of opposite polarity. This attenuation of biological response by reversal of the electric field direction has been reported with pulse durations from 60 ns to 900 ns for a wide range of endpoints, and it is not observed with conventional electroporation pulses of much longer duration ($> 100 \mu\text{s}$) where pulses are additive regardless of polarity. The most plausible proposed mechanisms involve the field-driven migration of ions to and from the membrane interface (accelerated membrane discharge). Here we report 2 ns bipolar pulse cancellation, extending the scale of previously published results down to the time required to construct the permeabilizing lipid electropores observed in molecular simulations. We add new cancellation endpoints, and we describe new bipolar pulse effects that are distinct from cancellation. This new data, which includes transport of cationic and anionic permeability indicators, fluorescence of membrane labels, and patterns of entry into permeabilized cells, is not readily explained by the accelerated discharge mechanism. We suggest that multi-step processes that involve first charged species movement and then responses of cellular homeostasis and repair mechanisms are more likely to explain the broad range of reported results.

1. Introduction

1.1. Electroporation — unanswered questions

Membrane permeabilization by pulsed electric fields enables biomedical and industrial applications like electrochemotherapy [1], irreversible electroporation [2], and food extraction and processing [3,4], despite the lack of a solid biophysical understanding of the phenomenon. Studies spanning decades have provided important insights [5–9], but procedures and protocols are still optimized empirically, because the underlying mechanisms have not been established, and robust, *predictive* models do not exist.

Recently a new puzzle was added to the stubborn mysteries of electroporation — nanosecond bipolar pulse cancellation, the elimination of the effects of a unipolar pulse by a subsequent pulse of opposite polarity. Bipolar pulse cancellation was first demonstrated with propidium permeabilization, increases in intracellular calcium concentration, and cell killing [10,11]. The universality of the phenomenon has since been established with reports of bipolar pulse cancellation with a variety of cell types, pulse durations, pulse shapes, and measurement endpoints [12–17].

Nanosecond bipolar pulse cancellation is unexpected because the annihilation or attenuation of the effects of pulse exposure by

additional pulses of opposite polarity runs contrary to what is observed in conventional electroporation protocols, which use pulses of microsecond or millisecond duration. With these longer pulses, a second pulse is additive, regardless of its polarity [18,19]. An even more puzzling feature of this phenomenon is that cancellation is observed even with delays as long as $50 \mu\text{s}$ between the two phases of a nanosecond bipolar pulse, a period much longer than the membrane charging-discharging time, which is not more than a few microseconds even for large cells [10,15,17].

Traditional representations of electroporation, including recent versions of the standard model [20,21] that explicitly incorporate the sub-microsecond time scale, do not predict this cancellation effect in the nanosecond pulse regime. Pore dynamics in the standard model are based on the mechanical energies of hydrophobic and hydrophilic pores resulting from the interplay of surface and line tensions in a lipid bilayer [22–25]. Increasing the transmembrane potential lowers the energy barrier for formation of a hydrophilic pore [20,21]. Within a few nanoseconds after the pore formation barrier is overcome, the number of hydrophilic pores and the membrane conductance increase dramatically, and the membrane potential drops close to zero [26]. A second pulse (of the same or opposite polarity) arriving while the membrane is in this conductive state cannot induce a transmembrane potential and thus cannot change the number or the size of existing pores, and should

* Corresponding author.

E-mail address: esozer@odu.edu (E.B. Sözer).<https://doi.org/10.1016/j.bbamem.2019.03.019>

Received 14 December 2018; Received in revised form 5 March 2019; Accepted 28 March 2019

Available online 11 April 2019

0005-2736/ © 2019 The Authors. Published by Elsevier B.V. This is an open access article under the CC BY-NC-ND license (<http://creativecommons.org/licenses/by-nc-nd/4.0/>).

not, in the framework of these models, have an attenuating effect on membrane permeabilization-related endpoints.

1.2. Membrane charging and discharging in an external electric field

In a simplified electrophysiological model of a biological cell in an alternating electric field, the membrane can be capacitively charged from its normal, slightly negative transmembrane potential, $-V_{m,resting}$, to a suprphysiological voltage, $V_{m,induced}$, and then discharged, during the second phase of the alternating waveform, back to $-V_{m,resting}$ and further to $-V_{m,induced}$ [27,28]. The values of $V_{m,induced}$ and $-V_{m,induced}$ depend on the duration and magnitude of the phases of the applied electric field. It has been proposed that the second phase of a bipolar pulse, by rapidly discharging the membrane from $V_{m,induced}$ to $-V_{m,resting}$ (accelerated discharge, also called “assisted discharge”), could reduce or cancel effects resulting from the exposure of the cell to the suprphysiological $V_{m,induced}$ induced by the first phase [10].

The peak induced membrane potential, $V_{m,induced}$, for a given external electric field amplitude E_0 can be approximated at the electrode-facing poles of a spherical cell of radius r by the Pauly-Schwan equation [27]:

$$V_{m,induced} = \frac{3}{2}E_0r \quad (1)$$

V_m cannot increase without limit. When $|V_m|$ exceeds a critical value (which can be as low as 300 mV), the membrane becomes electrically conductive and permeable to ions and small molecules [29–32].

A critical assessment of the proposed accelerated (assisted)

discharge mechanism for bipolar pulse cancellation requires an analysis of the time course of membrane potential changes during pulse exposure. Assume an initial value $V_{m,0}$ for the transmembrane potential. Under the influence of a time-invariant external electric field with a magnitude that results in a peak membrane potential, $V_{m,induced}$, the time-dependent membrane potential V_m is given by the capacitive charging equation:

$$V_m(t) = V_{m,0} + (V_{m,induced} - V_{m,0}) \left(1 - \exp\left(-\frac{t}{\tau_m}\right) \right) \quad (2)$$

where t is the time after the electric field is applied and τ_m is the membrane charging time constant, which can be calculated from the intracellular and extracellular conductivities (σ_i and σ_e) and the thickness of the membrane, d_m [28]:

$$\tau_m = \frac{r\epsilon_m}{2d_m(\sigma_i\sigma_e/(\sigma_i + 2\sigma_e))} \quad (3)$$

Note that the kinetics of charging and discharging, and therefore the time course of an “accelerated discharge” and the effectiveness of cancellation, depend directly on the value of the membrane charging time constant with respect to external electric field duration (t/τ_m) and on the external electric field amplitude.

1.3. Pulse durations comparable to the membrane charging time τ_m

As a measure of the effectiveness of a given exposure, we can consider the integrated product of the transmembrane potential and the

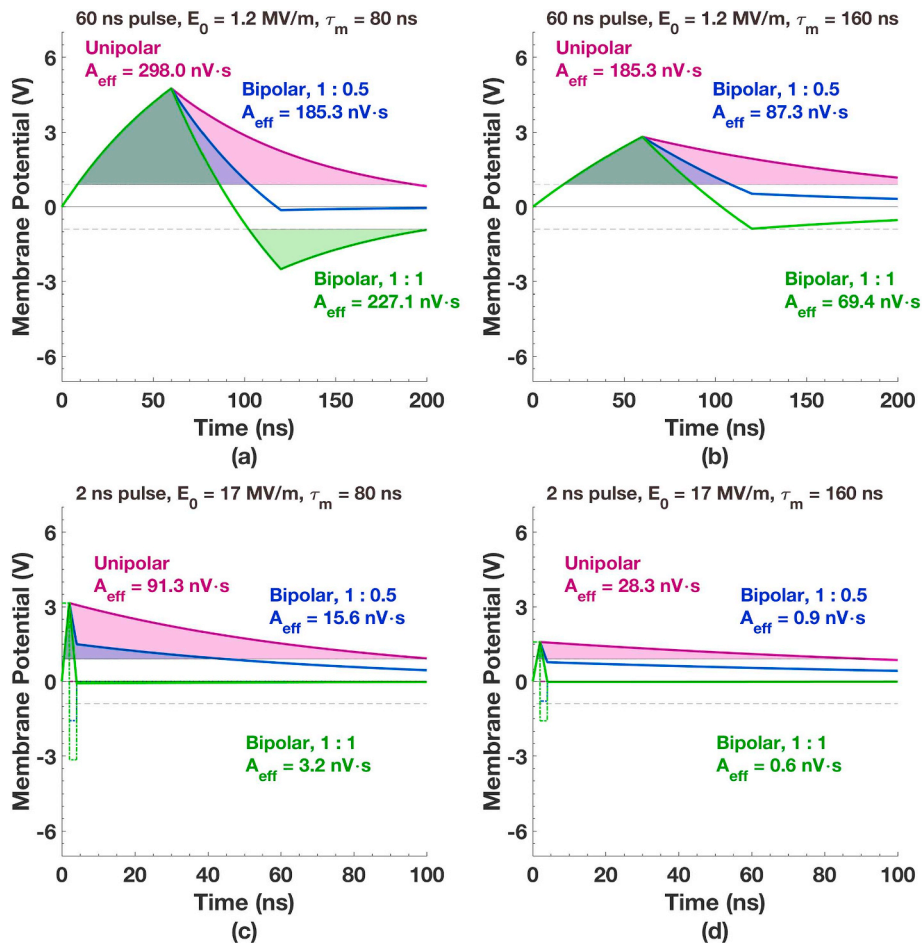


Fig. 1. Pulse-induced membrane charging and discharging after a unipolar pulse, asymmetric bipolar pulse (positive to negative phase ratio 1:0.5), and symmetric bipolar pulse (positive to negative phase ratio 1:1) with different pulse and membrane charging time constant parameters (a) 60 ns, 1.2 MV/m when $\tau_m = 80$ ns (b) 60 ns, 1.2 MV/m when $\tau_m = 160$ ns (c) 2 ns, 17 MV/m when $\tau_m = 80$ ns. (d) 2 ns, 17 MV/m, when $\tau_m = 160$ ns.

time during which the transmembrane potential is above some threshold, $V_{m,critical}$, that causes an effect. Assume $V_{m,critical} = 1$ V (on the high side of the range of reported experimental values). In Fig. 1a, the transmembrane potential driven by a rectangular, 60 ns, 1.2 MV/m unipolar pulse, used by Pakhomov et al. [10], discharges below $V_{m,critical}$ after about 200 ns, with a total dose of 298 nV·s. In this same example, the transmembrane potential is discharged to zero by an immediately following pulse of opposite polarity with an amplitude of 0.6 MV/m (positive to negative phase ratio 1:0.5), and a total dose of only 185 nV·s.

To understand this better, consider carefully the two bipolar analyses shown in Fig. 1a, which illustrates how a bipolar pulse with a second phase amplitude that is half that of the first phase discharges the membrane more effectively (lower Vt dose) than a bipolar pulse with first and second phases that are equal in amplitude. The lower amplitude second phase accelerates the discharging so that at the end of the second phase, membrane potential is below the critical potential (blue line in Fig. 1a). For the higher amplitude second phase, the larger discharge acceleration drives the induced membrane potential past the critical value at the opposite polarity from that induced by the first phase charging (green line, Fig. 1a), increasing the effective area of permeabilization relative to that produced by the lower amplitude second phase. For the smallest effective area, the second phase of the pulse must accelerate the discharging just the right amount so that at the end of the second phase, membrane potential is below the critical potential and stays there. If the acceleration of discharging driven by the second phase is too high, the membrane potential may go beyond the critical value in the opposite polarity, which also increases the effective area.

Pakhomov et al. [10] and other previous reports of nanosecond bipolar cancellation are based on cellular responses to 60–900 ns pulses, which have durations on the same order as the membrane charging time constant (~ 100 – 1000 ns) [10–12,14–17]. Using 60 ns pulses to induce YO-PRO-1 uptake, for example, Gianulis et al. [15] decreased the conductivity of the medium to prolong the discharge time by increasing τ_m , in order to see the effect on bipolar pulse cancellation. The expectation was that “increasing the time interval during which a polarity reversal can cancel the effects from the initial stimulus” would affect the time allowed between the two pulse phases for effective cancellation, but they “found that the time-dependence of bipolar cancellation was similar” for low- and high-conductivity media.

Approaching the question of the effect of medium conductivity (and membrane charging time) analytically, we plot in Fig. 1b V_m versus t for the same electric pulse used in Fig. 1a, but with the charging time constant doubled (by roughly a 10-fold change in extracellular conductivity). This relatively small change produces very different results shown in Fig. 1b. The reduction in Vt dose (“cancellation”) relative to the unipolar pulse exposure is roughly the same for the bipolar pulse with a second phase amplitude that is half that of the first phase and the bipolar pulse with first and second phases that are equal in amplitude. In general, for pulse durations comparable to the membrane charging time constant τ_m , changes in conditions that affect τ_m can produce large changes in the net exposure dose, Vt , contrary to experimental observations.

1.4. Pulse durations much shorter than the membrane charging time τ_m

To test further the accelerated discharge hypothesis, but without the complications and possible confounding effects of changing buffers or the high sensitivity to a small change in τ_m , we report here data from experiments using pulses at the short end of the nanosecond regime (pulse duration < 10 ns), where the pulse duration is significantly less than τ_m , and the results are relatively insensitive to τ_m . For example, a 2 ns, 17 MV/m bipolar pulse with equal amplitudes for each phase will induce a transmembrane potential that is discharged rapidly to 0 V even if the membrane charging time constant is doubled (Fig. 1c and d).

We observe 2 ns bipolar pulse cancellation in the myeloid cell line

U-937 with several endpoints: intracellular calcium concentration change, YO-PRO-1 influx, calcein efflux, and membrane labeling with FM 1-43. The calcein observations are the first report of cancellation of pulse-induced efflux from cells, and, at the same time, of cancellation of pulse-induced transport of an anionic, normally impermeant small molecule.

These 2 ns bipolar pulse results provide further evidence that the conditions required for cancellation by accelerated discharge are far too restrictive to account for the broad range of the conditions under which bipolar pulse cancellation is observed. In addition, we report here differences in spatial transport patterns and in volume regulation that point to previously unrecognized complexity in cellular responses to nanosecond unipolar and bipolar electrical stimuli.

2. Materials and methods

2.1. Cells

U-937 (human histiocytic lymphoma; ATCC CRL-1593.2) cells [33] were cultured in RPMI-1640 medium (Corning® glutagro™ 10-104-CV) with 10% fetal bovine serum (Corning, 35-010-CV) and 1% penicillin/streptomycin (10,000 U/mL penicillin and 10 mg/mL streptomycin) at 37 °C in a humidified, 5% CO₂ atmosphere.

2.2. Pulsed electric field exposure

2 ns, 17 MV/m pulses (HORUS pulse generator) or 2 ns, 42 MV/m (FID 10-2CN6V2) pulses were delivered to cells in suspension in cover glass chambers (Nunc™ Lab-Tek™ II) through parallel tungsten wire electrodes with 50–60 μm interelectrode gap [34]. Cells were observed at laboratory room temperature on the stage of a Leica TCS SP8 laser scanning confocal microscope. The HORUS pulse generator [35–37] delivers unipolar pulses of 2 ns full width at half maximum (FWHM) and bipolar asymmetric pulses of 1.8 ns FWHM each phase with negative phase amplitude 30% of the positive at a maximum electric field of 17 MV/m in our system. An FID GmbH pulse generator (model: FPG 10-1CN6V2, Burbach, Germany) provided 2 ns FWHM pulses for unipolar, asymmetric bipolar (negative phase 30% of positive), and symmetric bipolar (negative phase equal to positive phase) pulses. Waveforms can be seen in Fig. 2. Pulse parameters for each experiment were chosen for a detectable fluorescence change in our system with the lowest exposure dose that our electrode configuration/pulse generator can accommodate. For a summary table of results with pulse exposure parameters used, see supplementary material.

2.3. Molecular transport experiments

Cells were washed and suspended at approximately 5×10^5 cells/mL in fresh RPMI 1640 medium before all the experiments. 2 μM YO-PRO-1 and 20 μM FM 1-43 were added to the medium approximately 10 min before the recordings for the corresponding experiments. For calcium imaging and calcein efflux experiments, cells were incubated in fresh medium containing 1 μM Fluo-4-AM, and 0.25 μM calcein-AM for 15 min at 37 °C in a humidified, 5% CO₂ atmosphere, before being washed and resuspended in fresh RPMI 1640 medium.

2.4. Imaging

Laser scanning confocal fluorescence microscope images were captured (Leica TCS SP8) every second for two minutes (120 frames) from cell suspensions at room temperature in ambient atmosphere on the microscope stage. Confocal slices of 1 μm thickness around the widest cross-section of the cells were imaged for all experiments except for calcein efflux. For calcein efflux experiments, the pinhole was opened such that total fluorescence from the whole cell region was recorded, equivalent to a non-confocal fluorescence image acquisition [38].

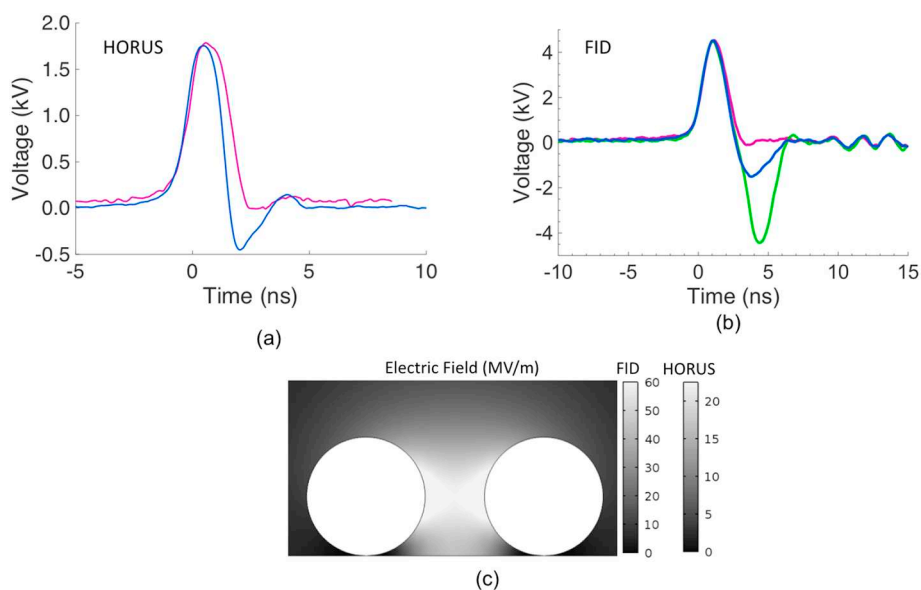


Fig. 2. Electric pulse shapes recorded during the experiments (a) from HORUS pulse generator with unipolar and bipolar asymmetric pulses (b) from FID pulse generator. (c) Peak electric field distributions in between electrodes.

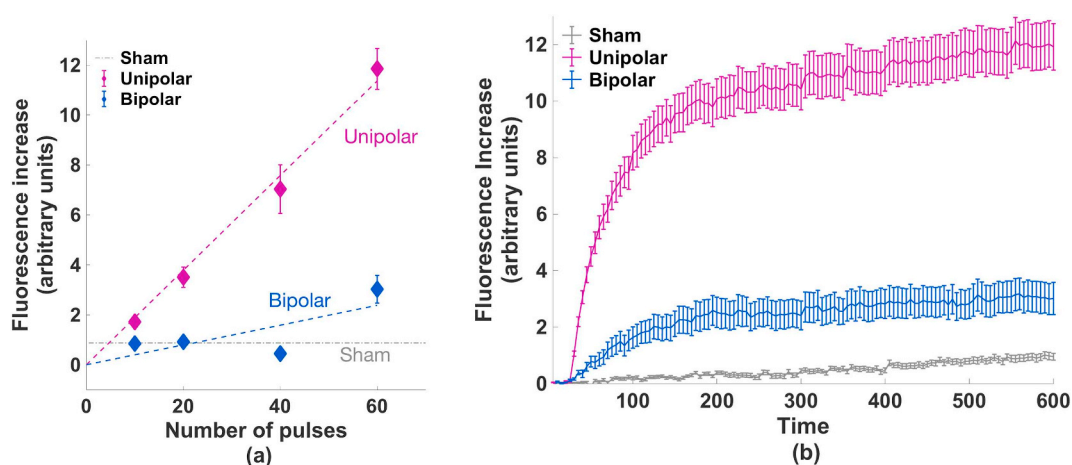


Fig. 3. (a) YO-PRO-1 uptake 10 minutes after exposure to unipolar and bipolar pulses (2 ns, 17 MV/m delivered at 1 kHz; 3 experiments, each with $n > 20$). (b) Time course of YO-PRO-1 uptake after 60 unipolar and bipolar pulses. Pulse waveforms in Fig. 2a.

2.5. Image processing

All cells visible in the microscope field between the electrodes were selected for fluorescence photometric image analysis before each pulse exposure. Fluorescence intensities of each region of interest were extracted using custom MATLAB routines. The following built-in MATLAB functions were used in custom image processing routines: 'imroi', for manually choosing regions of interest based on transmitted light image membrane boundaries; 'regionprops', for evaluating geometric properties of regions of interest. Image processing for YO-PRO-1 transport patterns was previously described [39]. Briefly, the cell areas in the images were divided into pixel rows parallel to the electrodes, and these rows were divided into three regions (anode-facing, middle, and cathode-facing), each with an equal number of rows. Analysis of polar behavior is based on the mean fluorescence intensity of each row for each region.

2.6. Cell volume measurements

Cell volumes were measured in medium containing 200 μ M calcein, as previously described [40]. Briefly, cell regions were isolated from z-

stack measurements in fluorescence images (where the cell outline is sharply defined by the fluorescence boundaries). The cell volume change ratio was calculated by normalizing the sum of total cell region areas from z-slices to the initial value of the same sum.

2.7. Statistical analysis

For all endpoints measured, at least three electric field exposures were performed with three different cell preparations and passages, and data was collected for 15–32 cells. The measurements are shown as the mean \pm standard error of the mean, and the number of cells for each experiment is indicated in figure captions.

3. Results

3.1. Bipolar cancellation can be observed with 2 ns pulses, consistent with previous reports with longer (> 60 ns) pulses

As pulse durations are decreased, a greater pulse amplitude is required, in general, to produce a given effect. With 17 MV/m unipolar and asymmetric bipolar pulses (Fig. 2a) we observed cancellation of

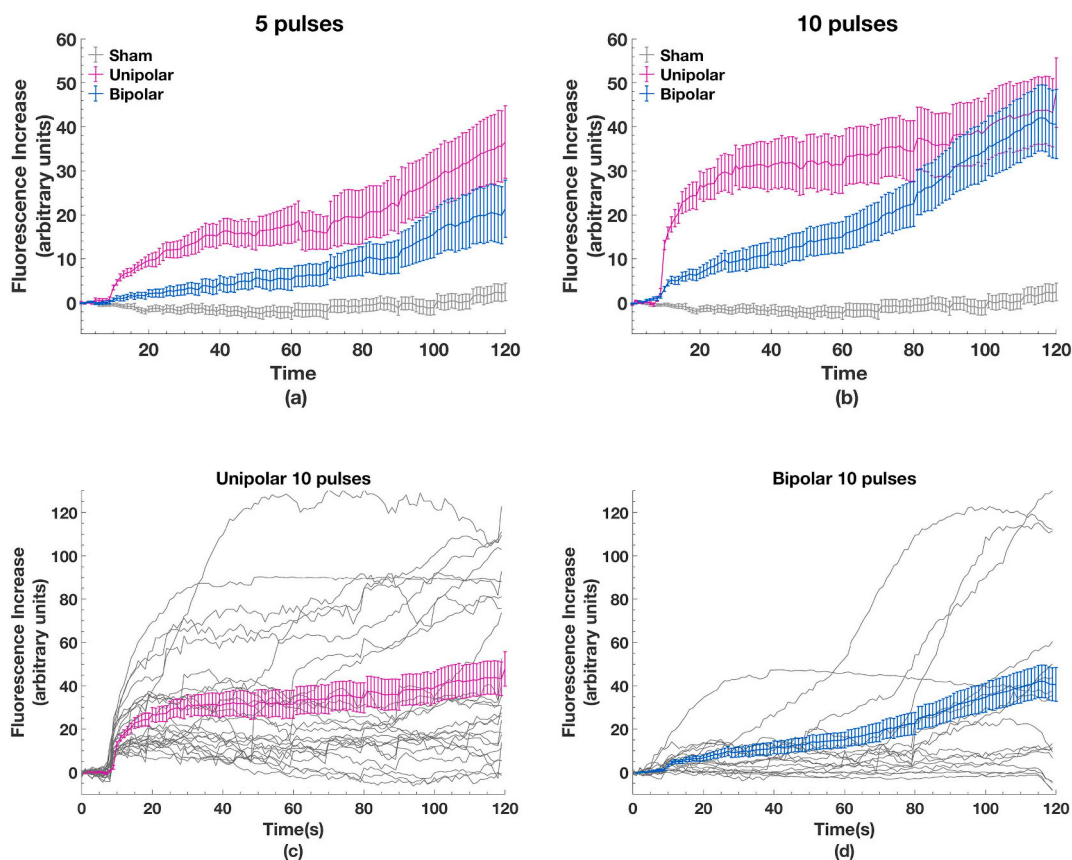


Fig. 4. Bipolar cancellation of intracellular calcium increase after 2 ns, 17 MV/m pulses at 1 kHz. (sham: mean of 10 cells) (a) 5 pulses (unipolar: mean of 32 cells, bipolar: mean of 29 cells), (b) 10 pulses (unipolar: mean of 25 cells, bipolar: mean of 17 cells), (c) individual traces from 10 pulse unipolar exposures in (b), (d) individual traces from 10 pulse bipolar exposures in (b).

pulse-induced YO-PRO-1 influx, intracellular calcium increase, and FM 1-43 fluorescence increase, consistent with results previously reported for 60, 200, and 300 ns pulses [10–12].

3.1.1. YO-PRO-1

2 ns unipolar pulse exposures (10, 20, 40, and 60 pulses) produce significantly greater YO-PRO-1 influx than sham exposures, linearly increasing with the number of pulses (Fig. 3a). Influx after bipolar pulse exposures is indistinguishable from sham exposures (i.e., cancellation was observed), except for 60 pulses (Fig. 3b). Exposures with fewer than ten pulses did not result in statistically significant uptake for either unipolar or bipolar pulses. We assume that we are at the limit of detectability for our system for this endpoint with these 2 ns, 17 MV/m pulses (maximum pulse amplitude with HORUS pulse generator in our setup, see [Materials and methods section](#) for details).

3.1.2. Intracellular calcium

2 ns unipolar pulses induce an immediate, sharp increase in cytosolic Ca^{2+} , much greater than the attenuated (“cancelled”) response to bipolar pulses (Fig. 4). Traces of calcium-associated fluorescence for individual cells (Fig. 4c and d) show a delayed calcium concentration increase in some cells, which has been attributed to calcium-induced calcium release [41]. At these very low pulse doses, where YO-PRO-1 influx is not detectable with our system, the calcium concentrations do not completely return to the basal intracellular levels, similar to what was reported for CHO cells, possibly because $[\text{Ca}^{2+}]_i$ is not high enough to activate plasma membrane Ca^{2+} -ATPase (PMCA) channels [41].

3.1.3. FM 1-43

The fluorescence of the cationic, amphiphilic dye FM 1-43 is enhanced in the hydrophobic interior of the cell membrane. 40, 2 ns, 17

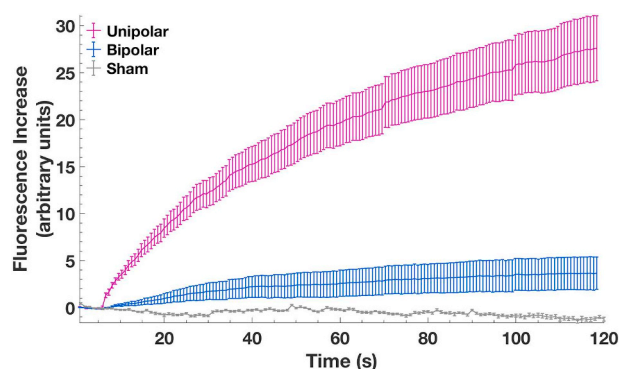


Fig. 5. Bipolar cancellation of FM 1-43 fluorescence increase after 40, 2 ns, 17 MV/m pulses at 1 kHz. $n > 16$ for each condition.

MV/m bipolar pulses caused an order of magnitude less FM 1-43 fluorescence increase than unipolar pulses of the same magnitude (Fig. 5). The pulse number in this case was chosen for a detectable fluorescence increase with bipolar pulses (Fig. 6).

3.2. 2 ns asymmetric bipolar pulses cause more cancellation (less YO-PRO-1 transport) than symmetric pulses

The accelerated membrane discharge hypothesis predicts varying the second phase amplitude should produce different amounts of cancellation. We tested this prediction with 2 ns pulses and YO-PRO-1 influx. To resolve the differences in YO-PRO-1 fluorescence intensity after bipolar pulse exposures with different second phase amplitudes, we

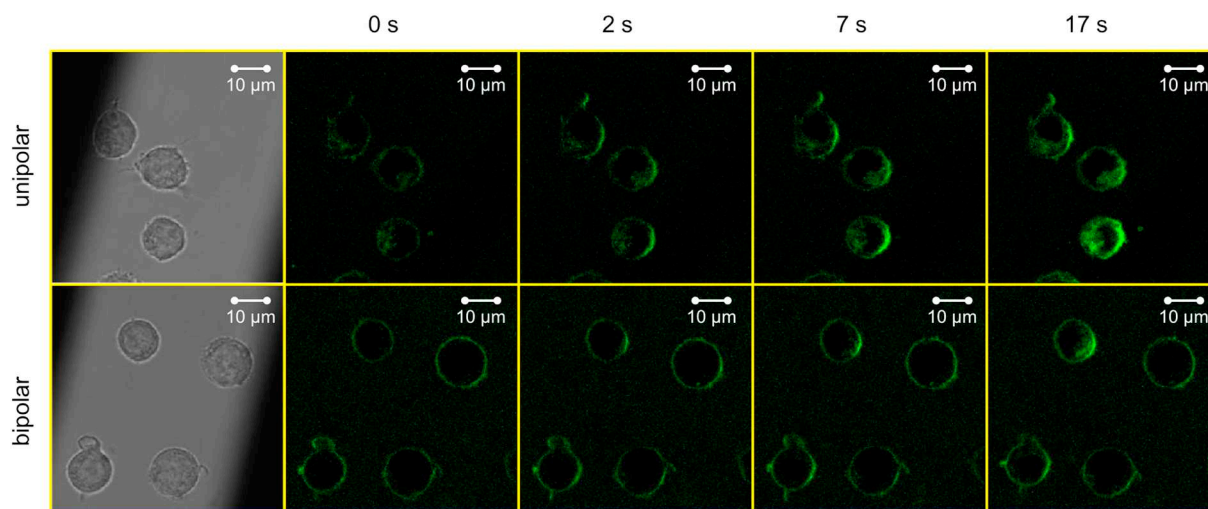


Fig. 6. Snapshots from FM 1-43 time series. Top row: unipolar, Bottom row: bipolar pulse. Pulse delivery at 0 s.

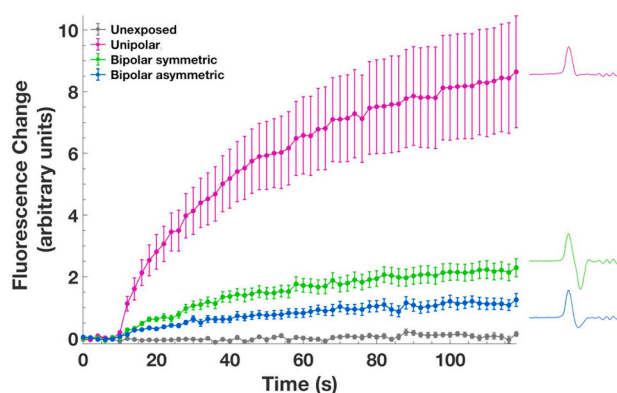


Fig. 7. YO-PRO-1 influx after 2 ns unipolar (magenta), bipolar asymmetric (blue), and bipolar symmetric (green) pulses. 10, 42 MV/m pulses delivered at 10 Hz. $n > 25$ for each condition.

increased the pulse amplitude to 42 MV/m. The results (Fig. 7) show that *asymmetric* bipolar pulses (positive to negative phase ratio 1:0.3) cause more cancellation than symmetric pulses (positive to negative phase ratio 1:1), consistent with previous experiments with longer, 230 ns, pulses [16].

3.3. YO-PRO-1 transport patterns are different after 2 ns unipolar and bipolar pulses

YO-PRO-1 transport into cells electropermeabilized with unipolar, sub-microsecond pulses was previously shown to have an asymmetric spatial distribution, with more transport observed at the pole of the cell facing the anode [39,42,43]. This unipolar pulse-induced transport pattern begins as a rapid fluorescence increase at the anodic side of the cell, then progresses to the middle and cathodic regions over a period of about 20 s [39].

YO-PRO-1 fluorescence immediately after a bipolar pulse exposure appears in roughly equal intensity on both anode and cathode sides of the cells for both symmetric and asymmetric 2 ns bipolar pulse exposures, and then advances uniformly toward the middle of the cell from both anode and cathode sides (Fig. 8). For bipolar pulse cellular fluorescence distributions, we call the side of the cell facing the ground electrode cathodic, and the side facing the active electrode (which can be positive or negative relative to the system ground) anodic.

When we adjust the dose (pulse number) for the cancellation effect so that unipolar and bipolar exposures induce roughly equal amounts of YO-PRO-1 influx (intracellular fluorescence), different spatial and temporal transport patterns are observed. Relative to the unipolar pulse exposure, the bipolar pulse exposure causes a slower fluorescence increase on the anodic pole of the cells, and a faster fluorescence increase on the cathodic pole (Fig. 8b, c).

3.4. Bipolar pulse cancellation of calcein efflux is similar to YO-PRO-1 influx

Bipolar cancellation of electropermeabilization in previous reports has always involved cationic species — Ca^{2+} , YO-PRO-1 $^{2+}$, FM 1-43 $^{2+}$, and propidium $^{2+}$ [10–12,15,16] — each of which binds to a greater or lesser extent to cell membranes [44–46, Supplementary information]. A recent report critically examined the importance of molecular charge in transport across electropermeabilized membranes. It showed that under the same electric pulse exposure conditions, the *efflux* of *anionic* calcein is comparable to the *influx* of cationic YO-PRO-1 and propidium, while calcein (*anionic*) *influx* is significantly less than the *influx* of the two *cationic* dyes [40].

To verify that bipolar pulse cancellation of membrane permeabilization is not dependent on the charge of the electro-transported material, we monitored efflux of calcein from cells in which the dye had been loaded using the membrane-permeant acetoxymethyl ester [40]. Bipolar pulse cancellation of calcein efflux was indeed observed, with asymmetric bipolar pulses more effective at cancellation than symmetric pulses (Fig. 9), consistent with our results for influx of the cationic dye YO-PRO-1 (Fig. 7) and with previous reports [16].

3.5. Cell volume changes after 2 ns unipolar and bipolar pulses

During calcein efflux experiments (Fig. 9), we noticed that the cell areas changed differently after unipolar and bipolar pulse exposures (Fig. 10a). Cell area increases after unipolar exposures, consistent with pulse-induced, osmotically driven, cell swelling [47–49], but cell area *decreases* after bipolar exposures, indicating more than simple “cancellation.”

To understand this better, we monitored cell volume changes with z-stack photometric analysis of cells in 200 μM calcein solutions after unipolar and bipolar pulse exposures that are equally permeabilizing to YO-PRO-1, since osmotically driven cell swelling is known to depend on permeabilizing stimulus dose [47–49]. We determined that 9, 2 ns 42 MV/m unipolar pulses cause approximately the same YO-PRO-1 uptake

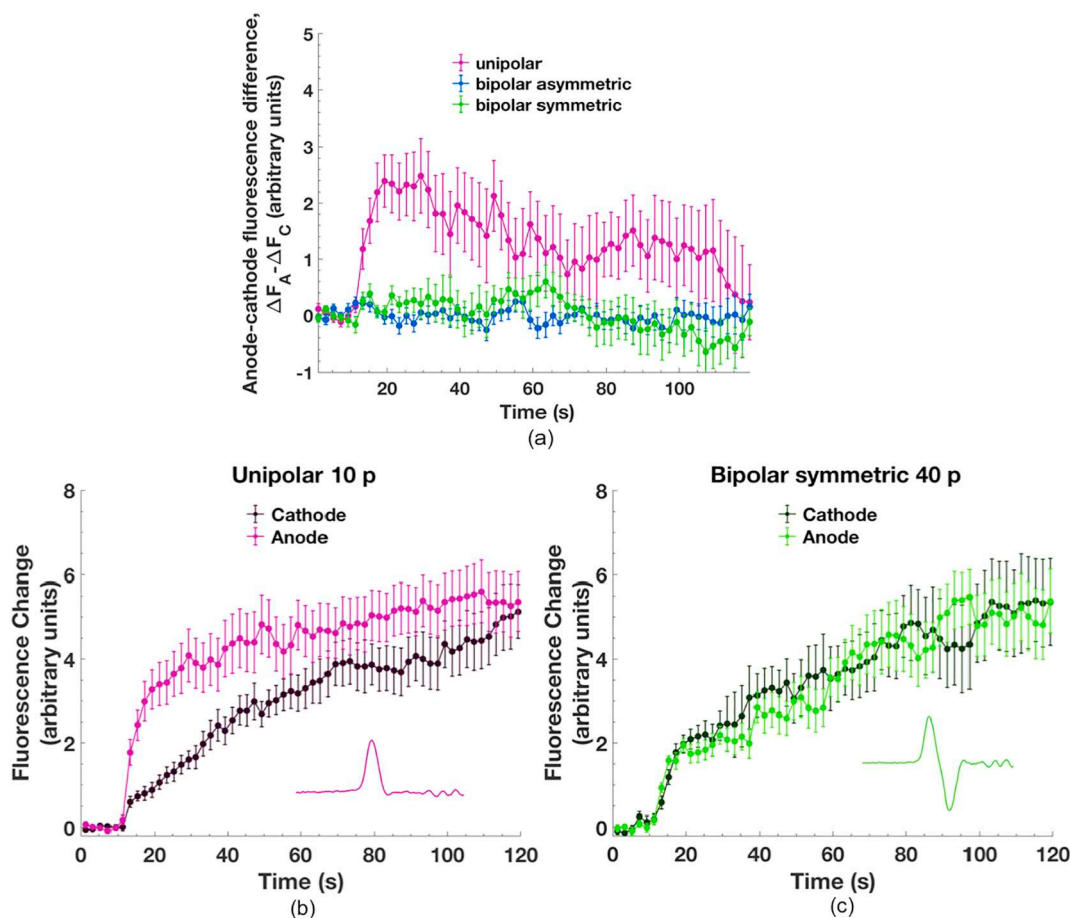


Fig. 8. YO-PRO-1 fluorescence at the anode- and cathode-facing sides of the cells. (a) Difference between anodic and cathodic fluorescence after 10, 42 MV/m pulses at 10 Hz shows the dominance of anodic side YO-PRO-1 influx after unipolar (magenta) pulses, and approximately equal intensity patterns at the anodic and cathodic poles after bipolar pulses (blue and green, asymmetric and symmetric). (b, c) Patterns after equally permeabilizing doses of (b) unipolar (magenta) and (c) bipolar (green) (10 and 40, respectively, 42 MV/m pulses delivered at 10 Hz) are shown at the anodic (active electrode) pole and at the cathodic (ground electrode) pole of the cells. $n > 23$ for each condition.

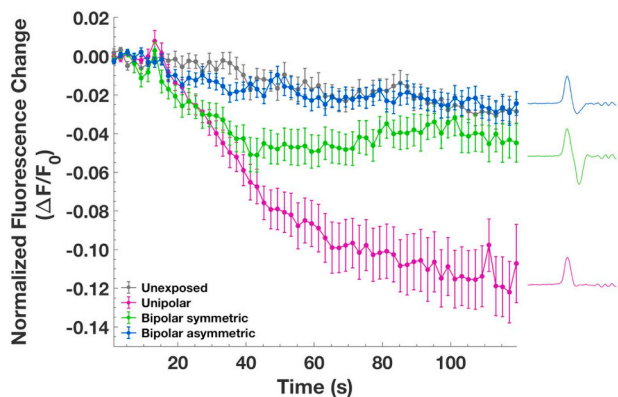


Fig. 9. Calcein efflux after 40, 2 ns, 42 MV/m unipolar, symmetric bipolar, and asymmetric bipolar pulses delivered at 10 Hz. $n > 20$ for each condition.

as 40 bipolar pulses at the same electric field (Supplementary Fig. S1). Although 40 unipolar pulses cause clear swelling (Fig. 10a), no volume change is observed with 9 unipolar pulses when compared to a sham exposure (Fig. 10b). 40 bipolar pulses, in contrast, cause significant shrinking (Fig. 10b). 2 ns bipolar pulses thus not only cancel the unipolar pulse-induced cell swelling, but also cause an unexpected and unexplained reduction in cell volume.

4. Discussion

4.1. Bipolar cancellation occurs with 2 ns pulses, and cancellation is more effective with asymmetric bipolar pulses

We have demonstrated here that nanosecond bipolar pulse cancellation occurs with pulses as short as 2 ns, and that asymmetric pulses (second phase amplitude lower than first phase) cancel more effectively than symmetric pulses, as has been shown previously for 60 ns and longer pulses. The experiments described here thus put new constraints on plausible mechanisms for bipolar pulse cancellation. 2 ns is roughly the time it takes to construct a lipid electropore, assumed to be the first and fundamental permeabilizing structure formed in biological membranes under electrical stress [50], and it is much shorter than the time required for even the fastest biochemical reactions or for large conformational changes in biomolecules. The process that triggers “cancellation” of membrane permeabilization and the other endpoints reported for this phenomenon must occur in 2 ns or less.

A reversal of the field does not reverse lipid electropore formation in molecular simulations [51]. A spectral analysis of bipolar pulse cancellation suggests that charged species movement and associated capacitive charging of the cell membrane is a major component of the mechanism underlying nanosecond bipolar pulse cancellation [13], consistent with the accelerated membrane discharge hypothesis. To evaluate this hypothesis more directly, we developed an analysis based on a dielectric shell model of the cell [27] to track the evolution of the

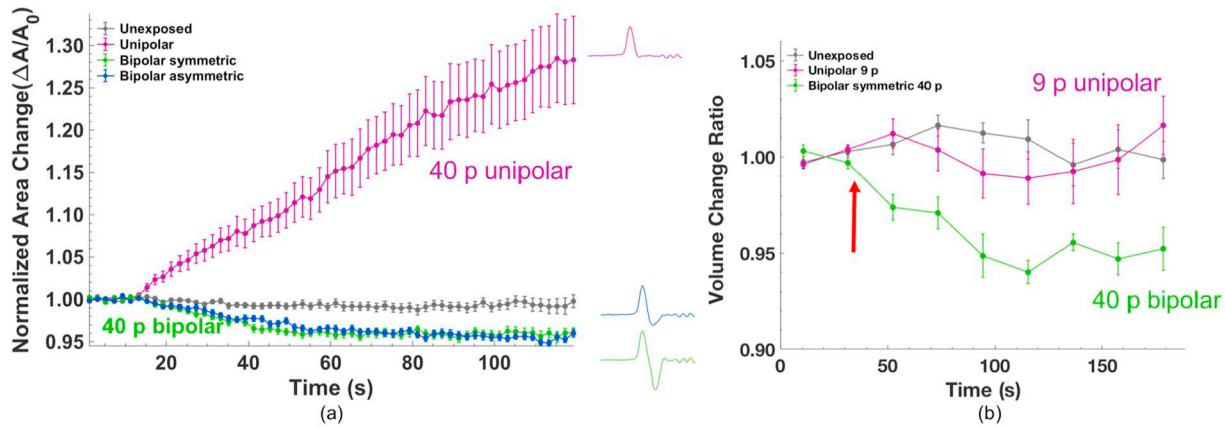


Fig. 10. (a) Cell area change after 40, 2 ns, 42 MV/m pulses delivered at 10 Hz at $t = 10$ s. $n > 20$ for each condition. (b) Volume change ratio after equally permeabilizing (YO-PRO-1) pulse exposures: 9, 2 ns, 42 MV/m unipolar pulses at 10 Hz (magenta) and 40, 2 ns, 42 MV/m bipolar pulses at 10 Hz (green). The red arrow indicates the time of the pulse exposure. $n > 15$ for each condition.

transmembrane potential (V_m) under the conditions of the experiments that produced the results plotted in Fig. 7. This analysis, defined by Eqs. (1)–(3), shown in Fig. 11a, indicates that asymmetric bipolar pulses (positive to negative phase ratio 1:0.3) should be *more* effective than symmetric pulses (positive to negative phase ratio 1:1), contrary to what we actually observe.

For Fig. 11(a) we assumed that the induced transmembrane potential, V_m , can increase without limit, which is not true for a biological membrane. When V_m reaches a high enough value, the membrane permeabilizes, and the membrane conductance increases, effectively clamping the maximum value of V_m . If we assume, arbitrarily, that $V_{m,max} = 4.5$ V, for example, we get the charging/discharging picture plotted in Fig. 11(b). As a rough measure of the effectiveness of a given exposure, we compute the area under the V_m versus t curve where $V_m > 1$ V, a nominal value for the transmembrane potential that causes permeabilization, and then from Fig. 11b we predict results consistent with the experimental observations of Fig. 7. Note that with these assumptions, the clamping of the membrane potential drives the membrane potential to higher negative values for symmetric bipolar pulse (Fig. 11b). Does this mean we arrived at $V_{m,max}$ values that are inconsistent with experimental observations? To assess this, we look at previously published data of bipolar cancellation with changing second phase amplitudes.

If we make similar calculations for V_m using experimental conditions from an earlier report (230 ns, 900 kV/m pulses, CHO cells [16], shown in Fig. 12, the prediction (more effective cancellation with symmetric than with asymmetric pulses) again runs contrary to the

experimental findings. Compare panels b (experimental) and d (model) in Fig. 12. Note that this exercise in plotting the charging/discharging dynamics and calculating the corresponding effective areas makes it clear that charging by the second phase of a bipolar pulse in the opposite direction can easily end up in a larger effective area under a wide range of electrical parameters, which is not ever observed in any of the reported experiments under many varying conditions for pulses of durations from 2 ns to 900 ns pulses [10–12,14–17].

This analysis demonstrates clearly that accelerated membrane discharge alone cannot explain bipolar pulse cancellation. The sensitivity of membrane charging and discharging to pulse duration, second phase amplitude, membrane charging time constant, and maximum transmembrane potential disallows this simple explanation for the wide range of conditions under which bipolar pulse cancellation has been observed [10–12,14,16,17]. The results shown here for 2 ns pulse exposures, where the pulse duration is significantly smaller than the membrane charging time, provides strong new evidence for this argument.

To understand bipolar pulse cancellation, it will surely be necessary to go beyond the simple electrophysiological model of the cell to represent the chemical and biological complexity of the plasma membrane and to take into account the multiple avenues for molecular transport across the membrane. Hypothetical mechanisms should be multi-step and multi-dimensional, *beginning* with charged species movement and membrane capacitive charging (physics), and then *progressing* to cellular homeostatic and repair responses to membrane permeabilization (biology). These may include maintenance of osmotic balance and

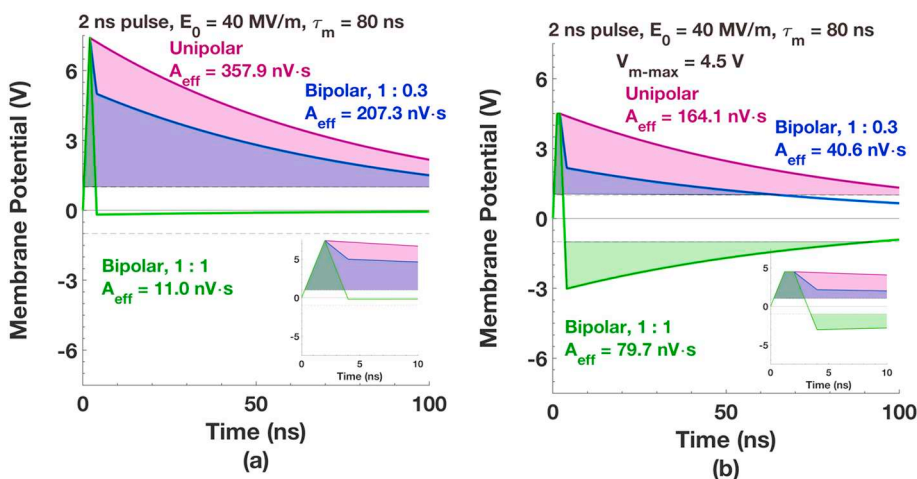


Fig. 11. Calculated U-937 cell membrane charging and discharging for 2 ns, 40 MV/m pulses: unipolar, asymmetric bipolar (positive to negative phase ratio 1:0.3), symmetric bipolar (positive to negative phase ratio 1:1) (a) without any limit on membrane potential amplitude (b) with $V_{m,max} = 4.5$ V. Insets show first 10 ns of the dynamics.

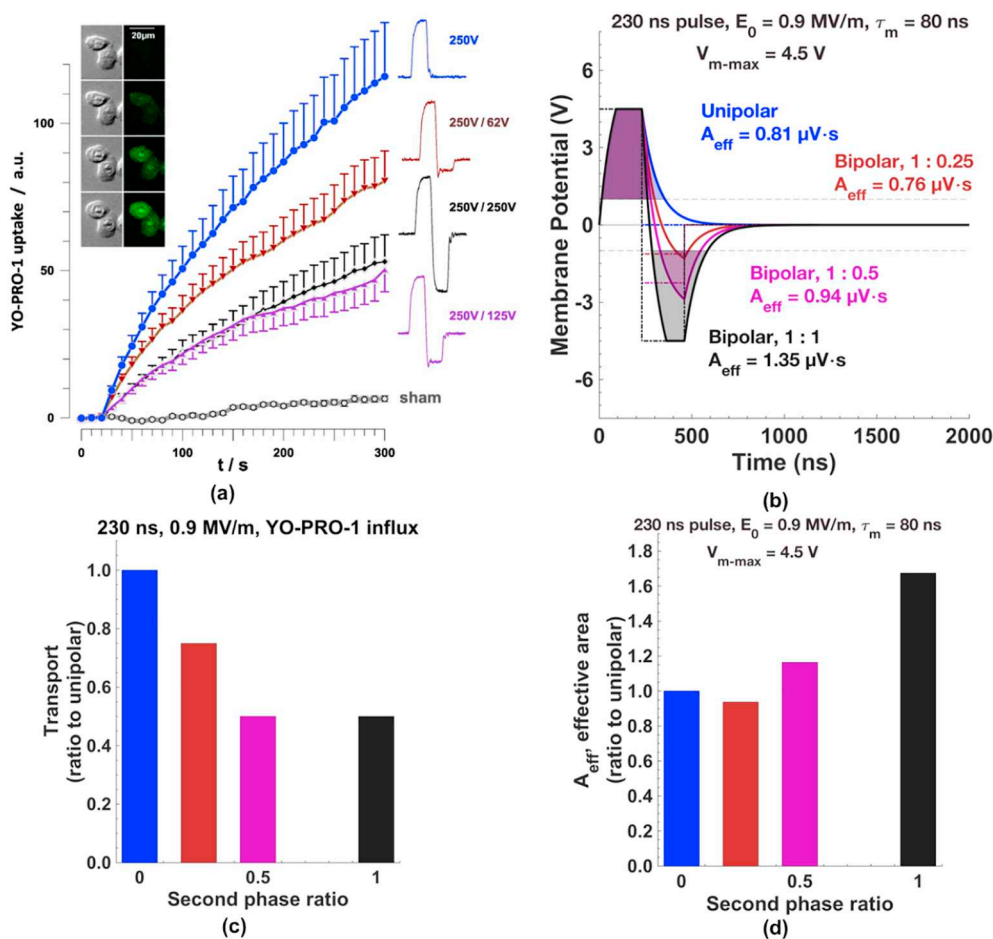


Fig. 12. (a) Experimental results of YO-PRO-1 influx into CHO cells after 230 ns bipolar pulses of varying second phase amplitude, from Pakhomov et al. (b) Calculated membrane charging and discharging for pulse exposures in (a), with $V_{m,max} = 4.5$ V. (c) Mean values of experimental results shown in (a) at 60 s into the recording. (d) Integrated values of effective area in (c).

membrane resting potential after stress-induced transport of Ca^{2+} , Na^+ , and K^+ , volume regulation, recovery or repair of voltage-sensitive membrane proteins, restoration of ATP and other metabolite levels, membrane repair, and other components of the electropermeome [46].

4.2. Bipolar pulse cancellation of anionic calcein efflux is similar to cationic YO-PRO-1 influx

Previously we have shown quantitatively that for a given pulse dose the electropermeabilization-induced influx of calcein is much less than the influx of YO-PRO-1, and that the efflux of calcein from pre-loaded cells under the same conditions is comparable to the influx of YO-PRO-1 [40]. From the new observation reported here that bipolar pulse cancellation of calcein efflux is comparable in magnitude to cancellation of YO-PRO-1 influx, we conclude that neither absolute charge nor direction of transport nor relative tendency to bind to or interact with the cell membrane (Supplementary Fig. S2) contributes significantly to the mechanism of bipolar pulse cancellation.

4.3. YO-PRO-1 transport patterns are different for 2 ns bipolar and unipolar pulse exposures

Analysis of transmembrane transport patterns for YO-PRO-1 following unipolar and bipolar pulse exposures shows that bipolar pulse cancellation of total molecular transport is not simply a uniform attenuation of the localized unipolar pulse transport pattern (anode-

dominant). Bipolar pulse exposures cause localized transport patterns distinct from unipolar pulse exposures, as was also shown with 900 ns pulses [14]. Electrically, when we switch the polarity of the pulses we are switching the cathodic and anodic pole of the cells. As one might expect, this switching of the poles results in equivalent transport at both poles (no anode-dominant pattern).

One potential explanation for cancellation of unipolar pulse-induced transport asymmetry can be found in standard (classical) models of electroporation [20,21]. While these models fail to predict the nanosecond bipolar pulse cancellation of total transport, mechanistic components in them may help to explain parts of the cancellation puzzle. The models predict that a high-amplitude electric pulse causes rapid pore formation, initially at the anodic pole of the cells. Pore formation is accompanied by an increase in conductance and a concomitant decrease in the local transmembrane potential, which limits pore size expansion [52]. This results in different pore formation dynamics on the cathodic side of the cell, where the induced transmembrane potential reaches higher values and produces larger but fewer pores, and is consistent with experimental studies with microsecond and millisecond duration pulses [53], which are “long” compared to plasma membrane discharge and pore creation and expansion times [7,50].

The situation is different for nanosecond pulse exposures, where the pulse duration is comparable to or much less than the characteristic times for membrane discharge and pore formation and expansion. Given these conditions it is reasonable to expect that unipolar pulses

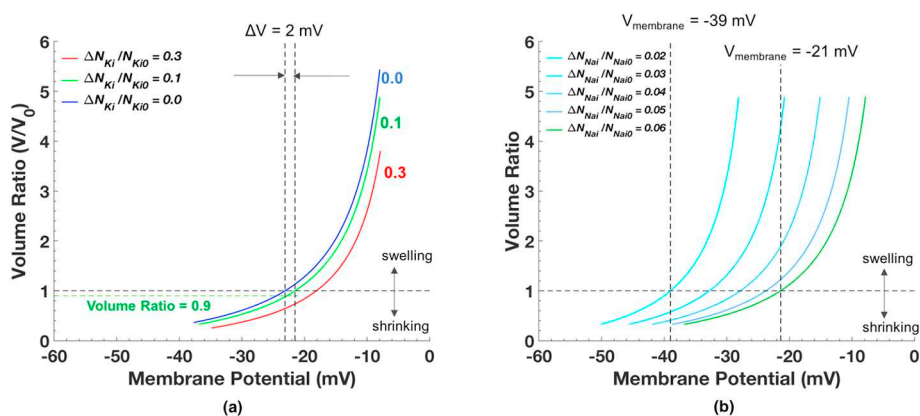


Fig. 13. Change in volume of an electropermeabilized cell versus membrane potential (a) for fractional changes in intracellular K⁺ 0.0 (blue), 0.1 (green), and 0.3 (red) (b) for fractional changes in intracellular K⁺ 0.1, and intracellular Na⁺ 0.02 to 0.05 (blue) and 0.06 (green). Green lines indicate the same condition in (a) and (b). Details can be found in the supplementary information.

will produce small anodic pores that continue to expand during the hundreds of nanoseconds or more that it takes to discharge the membrane. For very short (symmetric) bipolar pulses on the other hand, combining this scheme with our analysis in the Introduction, small pores will form at both poles of the cells, but they will not expand because the membrane has been discharged (Fig. 1c, d).

4.4. 2 ns bipolar and unipolar pulses affect cell volume differently

Nanosecond bipolar pulses do not simply cancel the cell swelling caused by a unipolar pulse. In fact, with some doses that are equally permeabilizing to YO-PRO-1, a unipolar pulse exposure leads to no detectable volume change, and a bipolar pulse exposure leads to cell *shrinking*. How can this be explained?

Cell volume, intracellular Na⁺, K⁺, and Cl⁻ concentrations, and membrane potential are tightly interconnected. In a living cell, any change in one of these factors (as a result of electropermeabilization or any membrane-perturbing event) will result in compensating changes in the others. A complete analysis of the inter-relationships of these cell characteristics must include at the same time an accounting of the effects of the membrane transport parameters that control both active and passive fluxes, for which numerical methods have been established [54–57].

From this perspective, we propose a mechanism that will result in different cell volumes after exposure to unipolar and bipolar pulses that cause a similar amount of total membrane permeabilization (based on YO-PRO-1 influx), but different post-exposure membrane potentials.

1. After electric field exposure the membrane is permeabilized, resulting in K⁺ efflux driven by the intracellular:extracellular K⁺ concentration gradient.
2. The intracellular K⁺ concentration momentarily decreases, with an associated partial depolarization of the membrane (membrane potential moves toward 0 mV).
3. a. For unipolar pulse exposures, membrane discharging takes longer (Fig. 1), allowing pore expansion and continuation of K⁺ efflux. The increased relative permeability of Na⁺ and Cl⁻ and the loss of intracellular K⁺, result in sustained partial membrane depolarization and osmotic imbalance, water *influx*, and cell swelling.
3. b. For bipolar pulse exposures, membrane potential discharging is faster (accelerated discharge), resulting in smaller pores and an associated smaller relative permeability of Na⁺, which interacts more with the lipid bilayer interface than do K⁺ and Cl⁻ [58–62]. This enables quicker recovery of physiological membrane potentials and intracellular [K⁺], leading to water *efflux* (compensating for the initial loss of intracellular K⁺ after permeabilization), and the cell shrinks. (Cf. Fig. 13 and further explanation below.)

In other words, we propose that the different sizes of permeabilizing

structures induced by unipolar and bipolar pulses (larger structures for unipolar pulses, which have longer discharge times, smaller for bipolar pulses, which have shortened discharge times) result in different permeabilities of Na⁺ relative to K⁺, leading to different sustained membrane potentials and cell volumes after the exposures.

Fig. 13a shows volume changes of an electropermeabilized cell as a function of membrane potential after K⁺ efflux, as predicted by the Nernst and Goldman-Hodgkin-Katz equations. (See the Supplementary Information for an explanation of this analysis of the effect of membrane potential on cell volume, including the effects of changes in K⁺, Na⁺ and Cl⁻ concentrations.) Under conditions that result in a 10% decrease in intracellular K⁺ (green lines in Fig. 13a and b), assuming transport of Na⁺ and Cl⁻ proportional to their concentration gradients (resulting in a 6% and 7% increase in intracellular Na⁺ and Cl⁻, respectively), a membrane potential change of only 2 mV (from -21 mV to -23 mV) is sufficient to drive volume regulation from “no volume change” to a 10% reduction in volume “shrinking”. Fig. 13b shows how varying the relative permeability of Na⁺ (compared to K⁺) — Na⁺ relative permeability is lower for very small pores than for larger pores, a nonlinear effect caused by interactions with the phospholipid bilayer interface that are greater for Na⁺ than for K⁺ [58–62] — affects the relationship between volume change and membrane potential. Smaller pore sizes result in membrane potentials closer to the physiological condition (farther from zero), and the volume ratio becomes more sensitive to changes in membrane potential.

5. Conclusions

2 ns pulses cause bipolar cancellation similar to that observed with pulse durations from 60 ns to 900 ns. The effectiveness of the cancellation of molecular transport of the fluorescent dyes YO-PRO-1 and calcein is greater when the amplitude of the second phase of the pulse is 30% of the amplitude of the first phase (compared to equal amplitude for both phases). The molecular transport pattern of YO-PRO-1 is different for unipolar and bipolar pulse exposures, consistent with the hypothesis that a bipolar pulse produces smaller pores than a unipolar pulse. We also critically examined the accelerated discharge hypothesis and showed that this hypothesis on its own does not predict many experimental results. Surprisingly, we observed a significant difference in volume regulation behavior after unipolar and bipolar pulses. Bipolar pulses, but not unipolar, cause shrinking in isosmotic, standard growth medium. This likely involves differences in membrane potential recovery resulting from the different sizes of the permeabilizing structures caused by unipolar and bipolar pulses. The results reported here extend bipolar pulse cancellation to very short duration pulses (2 ns), and they support the idea that pulsed electric field-facilitated molecular transport and its cancellation in cells involves more than the formation and closing of openings in the cell membrane.

Author contributions

EBS and PTV conceived and planned the experiments. EBS performed the experiments, the data analysis, and the analytical calculations. EBS and PTV wrote the manuscript.

Transparency document

The Transparency document associated with this article can be found, in online version.

Acknowledgements

EBS and PTV are supported by Air Force Office of Scientific Research (AFOSR) MURI grant FA9550-15-0517 on “Nanoelectropulse Induced Electromechanical Signaling and Control of Biological Systems” administered through Old Dominion University. PTV is also supported by AFOSR grant FA9550-14-1-0123 (a collaborative effort with FA9550-14-1-0018). Authors would like to thank Dr. Normand Leblanc and Dr. Christian Zemlin for useful discussions.

Appendix A. Supplementary data

Supplementary data to this article can be found online at <https://doi.org/10.1016/j.bbamem.2019.03.019>.

References

- [1] M. Marty, G. Sersa, J.R. Garbay, J. Gehl, C.G. Collins, M. Snoj, V. Billard, P.F. Geertsen, J.O. Larkin, D. Miklavcic, Electrochemotherapy—an easy, highly effective and safe treatment of cutaneous and subcutaneous metastases: results of ESOPE (European Standard Operating Procedures of Electrochemotherapy) study, *Eur. J. Cancer Suppl.* 4 (2006) 3–13.
- [2] R.V. Davalos, L.M. Mir, B. Rubinsky, Tissue ablation with irreversible electroporation, *Ann. Biomed. Eng.* 33 (2005) 223–231.
- [3] K. Dymek, P. Dejmeck, F.G. Galindo, Influence of pulsed electric field protocols on the reversible permeabilization of rucola leaves, *Food Bioprocess Technol.* 7 (2014) 761–773.
- [4] O. Parniakov, F.J. Barba, N. Grimi, L. Marchal, S. Jubeau, N. Lebovka, E. Vorobiev, Pulsed electric field assisted extraction of nutritionally valuable compounds from microalgae *Nannochloropsis* spp. using the binary mixture of organic solvents and water, *Innov. Food Sci. Emerg. Technol.* 27 (2015) 79–85.
- [5] I.P. Sugar, E. Neumann, Stochastic model for electric field-induced membrane pores electroporation, *Biophys. Chem.* 19 (1984) 211–225.
- [6] J. Teissie, M. Golzio, M.P. Rols, Mechanisms of cell membrane electro-permeabilization: a minireview of our present (lack of ?) knowledge, *Biochim. Biophys. Acta, Gen. Subj.* 1724 (2005) 270–280.
- [7] D.P. Tieleman, The molecular basis of electroporation, *BMC Biochem.* 5 (2004) 10.
- [8] P.T. Vernier, Nanoscale restructuring of lipid bilayers in nanosecond electric fields, in: A.G. Pakhomov, D. Miklavcic, M.S. Markov (Eds.), *Adv. Electroporation Tech. Biol. Med.*, CRC Press, 2010, pp. 161–174.
- [9] A.G. Pakhomov, O.N. Pakhomova, Nanopores: a distinct transmembrane passageway in electroporated cells, in: A.G. Pakhomov, D. Miklavcic, M.S. Markov (Eds.), *Adv. Electroporation Tech. Biol. Med.*, CRC Press, Boca Raton, 2010, pp. 178–194.
- [10] A.G. Pakhomov, I. Semenov, S. Xiao, O.N. Pakhomova, B. Gregory, K.H. Schoenbach, J.C. Ullery, H.T. Beier, S.R. Rajulapati, B.L. Ibey, Cancellation of cellular responses to nanoelectroporation by reversing the stimulus polarity, *Cell. Mol. Life Sci.* 71 (2014) 4431–4441.
- [11] B.L. Ibey, J.C. Ullery, O.N. Pakhomova, C.C. Roth, I. Semenov, H.T. Beier, M. Tarango, S. Xiao, K.H. Schoenbach, A.G. Pakhomov, Bipolar nanosecond electric pulses are less efficient at electroporation and killing cells than monopolar pulses, *Biochem. Biophys. Res. Commun.* 443 (2014) 568–573.
- [12] E.C. Gianulis, J. Lee, C. Jiang, S. Xiao, B.L. Ibey, A.G. Pakhomov, Electroporation of mammalian cells by nanosecond electric field oscillations and its inhibition by the electric field reversal, *Sci. Rep.* 5 (2015) 13818.
- [13] C. Merla, A.G. Pakhomov, I. Semenov, P.T. Vernier, Frequency spectrum of induced transmembrane potential and permeabilization efficacy of bipolar electric pulses, *Biochim. Biophys. Acta Biomembr.* 1859 (2017) 1282–1290.
- [14] C.M. Valdez, R.A. Barnes, C.C. Roth, E.K. Moen, G.A. Throckmorton, B.L. Ibey, Asymmetrical bipolar nanosecond electric pulse widths modify bipolar cancellation, *Sci. Rep.* 7 (2017) 16372.
- [15] E.C. Gianulis, M. Casciola, S. Xiao, O.N. Pakhomova, A.G. Pakhomov, Electroporation by uni- or bipolar nanosecond electric pulses: the impact of extracellular conductivity, *Bioelectrochemistry.* 119 (2018) 10–19.
- [16] A.G. Pakhomov, S. Grigoryev, I. Semenov, M. Casciola, C. Jiang, S. Xiao, The second phase of bipolar, nanosecond-range electric pulses determines the electroporation efficiency, *Bioelectrochemistry.* 122 (2018) 123–133.
- [17] C.M. Valdez, R. Barnes, C.C. Roth, E. Moen, B. Ibey, The interphase interval within a bipolar nanosecond electric pulse modulates bipolar cancellation, *Bioelectromagnetics.* (39) (2018) 441–450.
- [18] E. Tekle, R.D. Astumian, P.B. Chock, Electroporation by using bipolar oscillating electric field: an improved method for DNA transfection of NIH 3T3 cells, *Proc. Natl. Acad. Sci.* 88 (1991) 4230 LP–4234.
- [19] T. Kotnik, L.M. Mir, K. Flisar, M. Puc, D. Miklavcic, Cell membrane electro-permeabilization by symmetrical bipolar rectangular pulses: part I. Increased efficiency of permeabilization, *Bioelectrochemistry.* 54 (2001) 83–90.
- [20] K.A. DeBruin, W. Krassowska, Modeling electroporation in a single cell. I. Effects of field strength and rest potential, *Biophys. J.* 77 (1999) 1213–1224.
- [21] T.R. Gowrishankar, J.C. Weaver, Electrical behavior and pore accumulation in a multicellular model for conventional and supra-electroporation, *Biochem. Biophys. Res. Commun.* 349 (2006) 643–653.
- [22] J.D. Litster, Stability of lipid bilayers and red blood cell membranes, *Phys. Lett. A* 53 (1975) 193–194.
- [23] I.G. Abidor, V.B. Arakelyan, L.V. Chernomordik, Y.A. Chizmadzhev, V.F. Pastushenko, M.R. Tarasevich, Electric breakdown of bilayer lipid membranes I. The main experimental facts and their qualitative discussion, *Bioelectrochem. Bioenerg.* 6 (1979) 37–52.
- [24] L.V. Chernomordik, S.I. Sukharev, I.G. Abidor, Y.A. Chizmadzhev, Breakdown of lipid bilayer membranes in an electric field, *Biochim. Biophys. Acta Biomembr.* 736 (1983) 203–213.
- [25] R.W. Glaser, S.L. Leikin, L.V. Chernomordik, V.F. Pastushenko, A.I. Sokirko, Reversible electrical breakdown of lipid bilayers: formation and evolution of pores, *Biochim. Biophys. Acta Biomembr.* 940 (1988) 275–287.
- [26] R.S. Son, K.C. Smith, T.R. Gowrishankar, P.T. Vernier, J.C. Weaver, Basic features of a cell electroporation model: illustrative behavior for two very different pulses, *J. Membr. Biol.* 247 (2014) 1209–1228.
- [27] von H. Pauly, H.P. Schwan, Über die Impedanz einer Suspension von kugelförmigen Teilchen mit einer Schale, *Zeitschrift Für Naturforsch. B.* 14 (1959) 125–131.
- [28] T. Kotnik, G. Pucihar, Induced transmembrane voltage—theory, modeling, and experiments, in: A.G. Pakhomov, D. Miklavcic, M.S. Markov (Eds.), *Adv. Electroporation Tech. Biol. Med.*, CRC Press, 2010, pp. 51–70.
- [29] H.G.L. Coster, A quantitative analysis of the voltage-current relationships of fixed charge membranes and the associated property of “punch-through”, *Biophys. J.* 5 (1965) 669.
- [30] R. Benz, F. Beckers, U. Zimmermann, Reversible electrical breakdown of lipid bilayer membranes: a charge-pulse relaxation study, *J. Membr. Biol.* 48 (1979).
- [31] J. Teissie, T.Y. Tsong, Electric field induced transient pores in phospholipid bilayer vesicles, *Biochemistry.* 20 (1981) 1548–1554.
- [32] B. Gabriel, J. Teissie, Time courses of mammalian cell electroporation observed by millisecond imaging of membrane property changes during the pulse, *Biophys. J.* 76 (1999) 2158–2165.
- [33] C. Sundström, K. Nilsson, Establishment and characterization of a human histiocytic lymphoma cell line (U-937), *Int. J. Cancer* 17 (1976) 565–577.
- [34] Y.-H. Wu, D. Arnaud-Cormos, M. Casciola, L.M. Mir, V. Couderc, P.T. Vernier, Moveable wire electrode microchamber for nanosecond pulsed electric-field delivery, *IEEE Trans. Biomed. Eng.* 60 (2013) 489–496.
- [35] B. Vergne, V. Couderc, P. Leveque, A 30-kHz monocyclus generator using linear photoconductive switches and a microchip laser, *IEEE Photon. Technol. Lett.* 20 (2008) 2132–2134.
- [36] C. Merla, S. El Amari, M. Kanaan, M. Liberti, F. Apollonio, D. Arnaud-Cormos, V. Couderc, P. Leveque, A 10-Ω high-voltage nanosecond pulse generator, *IEEE Trans. Microw. Theory Tech.* 58 (2010) 4079–4085.
- [37] M. Kanaan, S.E. Amari, A. Silve, C. Merla, L.M. Mir, V. Couderc, D. Arnaud-Cormos, P. Leveque, Characterization of a 50-Ω exposure setup for high-voltage nanosecond pulsed electric field bioexperiments, *IEEE Trans. Biomed. Eng.* 58 (2011) 207–214.
- [38] T. Wilson, Resolution and optical sectioning in the confocal microscope, *J. Microsc.* 244 (2011) 113–121.
- [39] E.B. Sözer, C.F. Pocetti, P.T. Vernier, Asymmetric patterns of small molecule transport after nanosecond and microsecond electroporation, *J. Membr. Biol.* 251 (2018) 197–210.
- [40] E.B. Sözer, C.F. Pocetti, P.T. Vernier, Transport of charged small molecules after electroporation — drift and diffusion, *BMC Biophys.* 11 (2018) 4.
- [41] I. Semenov, S. Xiao, A.G. Pakhomov, Primary pathways of intracellular Ca²⁺ mobilization by nanosecond pulsed electric field, *Biochim. Biophys. Acta Biomembr.* 1828 (2013) 981–989.
- [42] P.T. Vernier, Y. Sun, M.A. Gundersen, Nanoelectropulse-driven membrane perturbation and small molecule permeabilization, *BMC Cell Biol.* 7 (2006) 37.
- [43] A. Bowman, O. Nesin, O. Pakhomova, A. Pakhomov, Analysis of plasma membrane integrity by fluorescent detection of Tl⁺ uptake, *J. Membr. Biol.* 236 (2010) 15–26.
- [44] V. Šator, M.A. Raftery, M. Martinez-Carrion, Propidium as a probe of acetylcholine receptor binding sites, *Arch. Biochem. Biophys.* 184 (1977) 95–102.
- [45] C. Altenbach, J. Seelig, Calcium binding to phosphatidylcholine bilayers as studied by deuterium magnetic resonance. Evidence for the formation of a calcium complex with two phospholipid molecules, *Biochemistry.* 23 (1984) 3913–3920.
- [46] E.B. Sözer, Z.A. Levine, P.T. Vernier, Quantitative limits on small molecule transport via the electropore — measuring and modeling single nanosecond perturbations, *Sci. Rep.* 7 (2017) 57.
- [47] O.M. Nesin, O.N. Pakhomova, S. Xiao, A.G. Pakhomov, Manipulation of cell volume and membrane pore comparison following single cell permeabilization with 60- and 600-ns electric pulses, *Biochim. Biophys. Acta Biomembr.* 1808 (2011) 792–801.
- [48] S. Romeo, Y.-H. Wu, Z.A. Levine, M.A. Gundersen, P.T. Vernier, Water influx and cell swelling after nanosecond electroporation, *Biochim. Biophys. Acta* 1828 (2013) 1715–1722.

- [49] E.B. Sözer, Y.-H. Wu, S. Romeo, P.T. Vernier, Nanometer-scale permeabilization and osmotic swelling induced by 5-ns pulsed electric fields, *J. Membr. Biol.* 250 (2017) 21–30.
- [50] Z.A. Levine, P.T. Vernier, Life cycle of an electropore: field-dependent and field-independent steps in pore creation and annihilation, *J. Membr. Biol.* 236 (2010) 27–36.
- [51] P.T. Vernier, Z.A. Levine, M.-C. Ho, S. Xiao, I. Semenov, A.G. Pakhomov, Picosecond and terahertz perturbation of interfacial water and electro-permeabilization of biological membranes, *J. Membr. Biol.* 248 (2015) 837–847.
- [52] W. Krassowska, P.D. Filev, Modeling electroporation in a single cell, *Biophys. J.* 92 (2007) 404–417.
- [53] E. Tekle, R.D. Astumian, P.B. Chock, Selective and asymmetric molecular transport across electroporated cell membranes, *Proc. Natl. Acad. Sci.* 91 (1994) 11512–11516.
- [54] E. Jakobsson, Interactions of cell volume, membrane potential, and membrane transport parameters, *Am. J. Physiol. Physiol.* 238 (1980) C196–C206.
- [55] J.A. Hernández, E. Cristina, Modeling cell volume regulation in nonexcitable cells: the roles of the Na⁺ pump and of cotransport systems, *Am. J. Physiol. Physiol.* 275 (1998) C1067–C1080.
- [56] J.A. Fraser, C.L.-H. Huang, A quantitative analysis of cell volume and resting potential determination and regulation in excitable cells, *J. Physiol.* 559 (2004) 459–478.
- [57] A.R. Kay, How cells can control their size by pumping ions, *Front. Cell Dev. Biol.* 5 (2017) 41.
- [58] M.E. Loosley-Millman, R.P. Rand, V.A. Parsegian, Effects of monovalent ion binding and screening on measured electrostatic forces between charged phospholipid bilayers, *Biophys. J.* 40 (1982) 221–232.
- [59] H. Binder, O. Zschörnig, The effect of metal cations on the phase behavior and hydration characteristics of phospholipid membranes, *Chem. Phys. Lipids* 115 (2002) 39–61.
- [60] T. Fukuma, M.J. Higgins, S.P. Jarvis, Direct imaging of lipid-ion network formation under physiological conditions by frequency modulation atomic force microscopy, *Phys. Rev. Lett.* 98 (2007) 106101.
- [61] A.A. Gurtovenko, I. Vattulainen, Effect of NaCl and KCl on phosphatidylcholine and phosphatidylethanolamine lipid membranes: insight from atomic-scale simulations for understanding salt-induced effects in the plasma membrane, *J. Phys. Chem. B* 112 (2008) 1953–1962.
- [62] M.-C. Ho, M. Casciola, Z.A. Levine, P.T. Vernier, Molecular dynamics simulations of ion conductance in field-stabilized nanoscale lipid electropores, *J. Phys. Chem. B* 117 (2013) 11633–11640.